Synthesis and luminescent properties of Mn-doped alpha-tricalcium phosphate

Lauryna Sinusaite[1], Andris Antuzevics[2], Anatoli I. Popov[2], Uldis Rogulis[2], Martynas Misevicius[1], Arturas Katelnikovas[1], Aivaras Kareiva[1], Aleksej Zarkov[1,*]

[1]*Institute of Chemistry, Vilnius University, Naugarduko 24, LT-03225 Vilnius, Lithuania*

[2]*Institute of Solid State Physics, University of Latvia, Kengaraga 8, LV-1063 Riga, Latvia*

*Corresponding author: E-mail: aleksej.zarkov@chf.vu.lt; +37062190153.

Abstract

In this work, a series of Mn^{2+}-doped α-tricalcium phosphate (α-TCP) powders was synthesized by wet co-precipitation method followed by high-temperature annealing and thermal quenching. It was shown that Mn^{2+}-doped α-TCP polymorph can be successfully synthesized with a doping level up to 1 mol%. All Mn-doped samples exhibited a broadband emission in the range from 525 to 825 nm with a maximum centered at around 630 nm. The highest emission intensity was observed for the sample with the highest content of Mn. The crystal structure and purity were evaluated by X-ray powder diffraction (XRD), Fourier-transform infrared (FTIR) and electron paramagnetic resonance (EPR) spectroscopies. Scanning electron microscopy (SEM) was used to investigate the morphological features of the synthesized products. Optical properties were investigated by means of photoluminescence measurements. Excitation spectra, emission spectra and decay curves of the samples were studied. Temperature-dependent photoluminescence measurements were performed as well.

Keywords: Tricalcium phosphate, α-TCP, Mn doping, luminescence.

1. Introduction

Synthetic calcium phosphates (CPs) are widely used for regenerative medicine purposes due to their biological properties and compositional similarity to natural human bone [1]. One of the most popular and frequently used CP is tricalcium phosphate (TCP, $Ca_3(PO_4)_2$). It has two polymorphs, which can be stabilized at room temperature, and both of them are used for biomedical applications as injectable bone fillers or ceramic substitutes [2, 3]. β-TCP is characterized by rhombohedral structure with the space group R3c (#161) and 5 inequivalent Ca sites, α-TCP crystallizes in the monoclinic crystal system with $P2_1/a$ space group (#14) and has 18 inequivalent Ca sites [4, 5]. α-TCP is assumed to be a high-temperature polymorph, which is usually synthesized by annealing of CP precursor mixture with Ca to P ratio 1.5:1 at temperatures above 1125 °C, which is the phase transition temperature for transformation from β- to α-TCP [6]. It is well known, that this phase transition is reversible and highly sensitive to the presence of impurities, most of smaller cations retard this transformation and stabilize β-TCP crystal phase [7-10]. Moreover, thermal quenching is frequently used to avoid undesired reversible transition and obtain single-phase α-TCP [11, 12].

Partial substitution of Ca ions by other biologically active cations is assumed to be a promising tool to superior biological properties of synthetic CPs [13-16]. It is also known that presence of foreign ions in CP matrix can modify significantly physicochemical, mechanical and anti-bacterial properties of materials, to promote changes in morphology, solubility and ion release kinetics [17]. Additionally, doping elements open new possibilities for applications of CPs as multifunctional materials. Optically active lanthanide ions and paramagnetic ions such as Gd^{3+} or Mn^{2+} make it possible to use these materials for bioimaging applications including fluorescence, magnetic resonance or multimodal imaging [18-21]. Due to complicated preparation of doped α-TCP, most of the works are focused on the synthesis and investigation of substituted β-TCP [22, 23] and very limited number on α-TCP [24-27]. Just recently, Luo et al. [28] suggested to use Eu doping for optical *in vivo* monitoring of biodegradation of α-TCP. Besides, α-TCP is considered as a promising host matrix for the synthesis of luminescent materials. Zhou et al. reported on cyan-emitting Eu^{2+}-doped α-TCP for potential

application in white emitting diodes [29]. Ji et al. [12] and Tong et al. [30] investigated luminescent properties of both TCP polymorphs partially substituted with Eu^{2+} ions.

Manganese is an essential element in human organism that plays an important role in bone development. It acts as a cofactor of several enzymes like glycosyltransferases which are involved in formation of bone and cartilage matrix [31, 32]. Furthermore, Mn^{2+} enhances the ligand binding affinity of integrin and activates osteoblast adhesion [33, 34]. Previous studies revealed that doping with Mn^{2+} ions resulted in improvements of bioactivity of calcium hydroxyapatite (HAp) coatings [35] and osteogenesis of CP-based cements [32]. Number of works on Mn-doped TCP were published, however all of them report on Mn-doped β-TCP [31, 32, 34, 36-38]. To the best of our knowledge, there are no papers studying Mn-doped α-TCP. The only report that briefly describes low-temperature metastable Mn-doped α-TCP is focused on thermodynamic stability and phase transition of TCP polymorphs [39].

At the same time Mn is also known for its optical properties and previously was incorporated into different hosts for the preparation of luminescent materials [40]. The electronic structure of Mn^{2+} ions allows shifting of their broadband emission from green to red depending on the crystal field strength of the host material [41]. Luminescent properties of Mn^{2+}-doped HAp and β-TCP were previously investigated by Lecointre et al. [42]. It was demonstrated that emission wavelength depends on the host material, orange emission peaked at 581 nm and red emission peaked at 645 nm were observed for HAp and β-TCP, respectively.

The main aim of this study was to investigate feasibility of the synthesis of Mn-doped α-TCP and to study its structural and luminescent properties. In order to do that, a series of α-TCP powders doped with different amounts of Mn^{2+} ions ranging from 0.2 to 1.0 mol% was synthesized by wet co-precipitation method followed by high-temperature thermal treatment. The crystal structure and purity were evaluated by X-ray powder diffraction, electron paramagnetic resonance and Fourier-transform infrared spectroscopies. Optical properties were investigated by means of photoluminescence measurements.

2. Materials and methods

2.1. Synthesis

Mn-doped α-TCP powders were synthesized by wet precipitation method. Calcium nitrate tetrahydrate ($Ca(NO_3)_2 \cdot 4H_2O$, ≥99%, Roth), manganese(II) nitrate tetrahydrate ($Mn(NO_3)_2 \cdot 4H_2O$, 98%, Alfa Aesar) and diammonium hydrogen phosphate ($(NH_4)_2HPO_4$, ≥98%, Roth) were used as starting materials. Total metal ions to phosphorous ratio was kept 1.5:1 for all samples. Firstly, 0.75 M Ca^{2+} and Mn^{2+} nitrate solution was prepared by dissolving metal salts in deionized water. Secondly, an appropriate amount of $(NH_4)_2HPO_4$ was separately dissolved in deionized water to obtain 0.5 M solution, to which concentrated ammonia solution (NH_4OH, 25%, Roth) was added in order to adjust pH value to 10. Next, metal ions solution was rapidly added to $(NH_4)_2HPO_4$ solution under constant stirring resulting in the instantaneous formation of precipitates. The reaction mixture was stirred for 10 minutes, afterwards precipitates were separated by vacuum filtering, washed with deionized water and ethanol. The obtained precipitates were dried at 50 °C overnight in the oven and ground in agate mortar. In order to obtain α-TCP phase, the precipitates were transferred to alumina crucible, annealed at 1250 °C for 12 h and rapidly cooled down on a metal plate.

2.2. Characterization

Powder X-ray diffraction (XRD) data were obtained using Ni-filtered Cu Kα radiation on a Bruker D8 Advance diffractometer with Bragg-Bretano focusing geometry and position sensitive LynxEYE detector. The data were collected within 2θ angle range from 10 to 110° (step width 0.01° and integration time 1.5 s). Fourier-transform infrared (FTIR) spectra were recorded in the range of 4000−400 cm^{-1} employing Bruker ALPHA ATR spectrometer with 4 cm^{-1} resolution. Morphology of the synthesized samples was investigated with a Hitachi SU-70 field-emission scanning electron microscope (FE-SEM). Elemental analysis of powders was carried out by inductively coupled plasma optical emission spectrometry (ICP-OES) using Perkin-Elmer Optima 7000DV spectrometer. The samples were dissolved in 5% nitric acid (HNO_3, Rotipuran® Supra 69%, Roth) and diluted to an appropriate volume. Calibration solutions were prepared by dilution of the stock standard solutions

(single-element ICP standards 1000 mg/L, Roth). Room temperature electron paramagnetic resonance (EPR) measurements were performed on Bruker ELEXSYS-II E500 CW-EPR system at X (9.5 GHz; 2 mW) and Q (33.9 GHz; 2 mW) microwave frequency bands. Magnetic field modulation amplitude was 0.2 mT. Spectra intensities for X-band EPR measurements were normalized to sample mass. Excitation and emission spectra were obtained on the Edinburgh Instruments FLS980 spectrometer equipped with double excitation and emission monochromators, 450 W Xe arc lamp, a cooled (-20 °C) single-photon counting photomultiplier (Hamamatsu R928), and mirror optics for powder samples. The photoluminescence (PL) emission spectra were corrected by a correction file obtained from a tungsten incandescent lamp certified by NPL (National Physics Laboratory, UK). When measuring excitation spectra (λ_{em}=670 nm), excitation and emission bandwidths were set to 1.60 and 5.00 nm, respectively. When measuring emission spectra (λ_{ex}=408 nm), excitation and emission bandwidths were set to 4.00 and 1.60 nm, respectively. For both measurements, step width was 1.00 nm and integration time was 0.2 s. The PL decay kinetics were measured on the same Edinburgh Instruments FLS980 spectrometer. Xe µ-flash lamp µF920 was used as an excitation source. Excitation wavelength was 408 nm while emission was monitored at 630 nm. The obtained data were fitted using the following equation:

$$I(t) = A + B_1 e^{(-t/\tau_1)} + B_2 e^{(-t/\tau_2)} \quad (1)$$

where $I(t)$ is luminescence intensity at a certain time t; A, B_1, B_2 corresponds to background and pre-exponential constants, respectively; τ_1, τ_2 are emission lifetime values. For temperature-dependent excitation and emission measurements, a cryostat MicrostatN from the Oxford Instruments had been applied the present spectrometer. Liquid nitrogen was used as a cooling agent. The measurements were performed at 77 K and at 100–500 K in 50 K intervals. Temperature stabilization time was 90 s and temperature tolerance was set to ±5 K. During the measurements dried nitrogen was flushed over the cryostat window to avoid the condensation of water at low temperatures on the surface of the window.

3. Results and discussion

The phase crystallinity and purity of all synthesized α-TCP powders were investigated by means of XRD analysis. The XRD patterns of CPs precipitates doped with different amounts of Mn^{2+} ions and annealed at 1250 °C for 12 hours are demonstrated in Fig. 1.

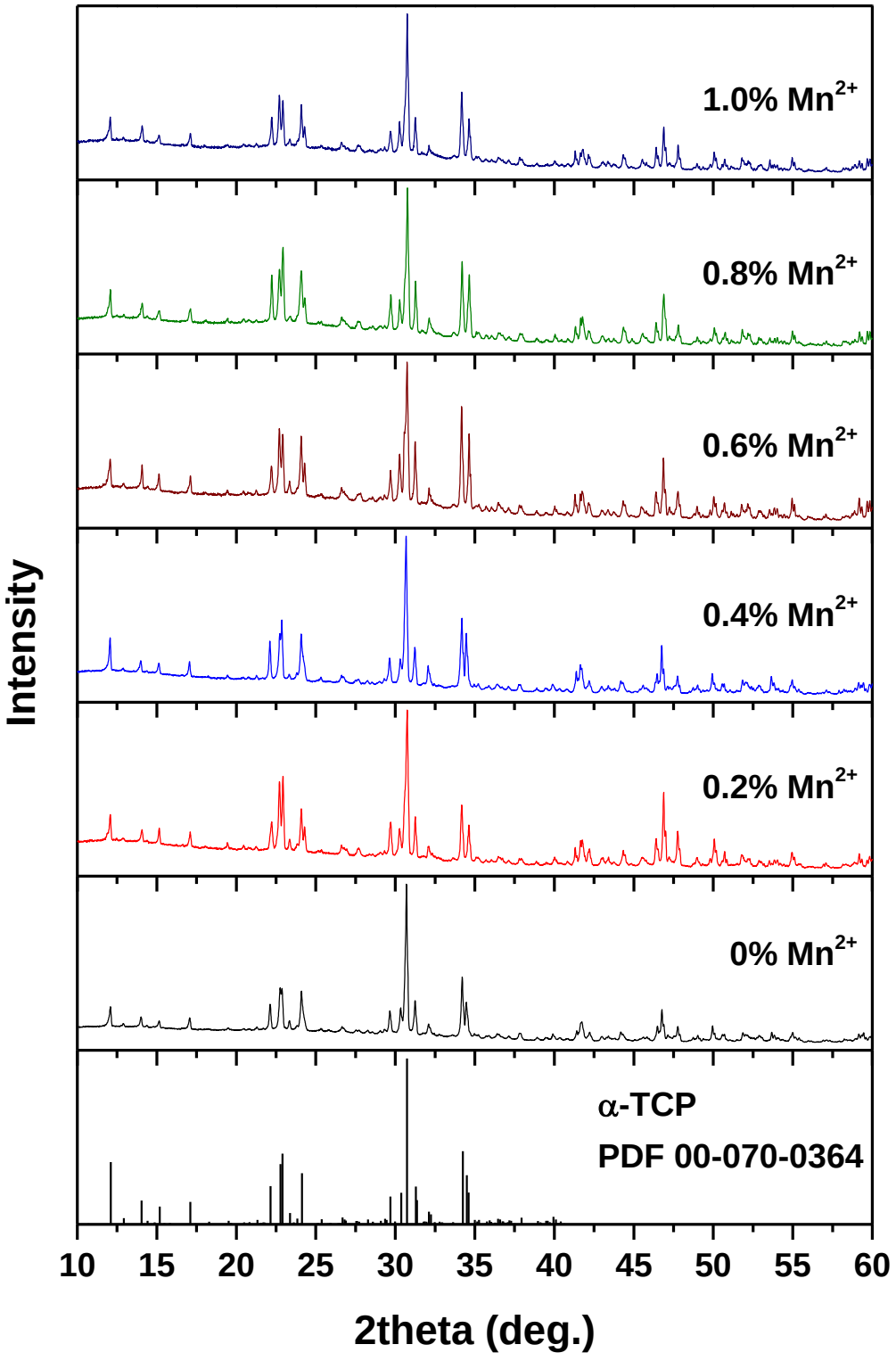

Fig. 1. XRD patterns of α-TCP powders doped with different amounts of Mn^{2+}.

The obtained results clearly indicate that after the thermal treatment α-TCP crystal phase was formed regardless of chemical composition of the samples. All diffraction peaks can be attributed to monoclinic $Ca_3(PO_4)_2$ and match well the standard XRD data (ICDD #00-070-0364). Not even traces of β-TCP polymorph were detected, indicating complete transformation of initial CP precursor to α-TCP and successful prevention of reversible phase transition, which was achieved by a thermal quenching. It should be noted, that attempts to synthesize α-TCP powders with higher content of Mn were unsuccessful and resulted in biphasic products containing certain amount of secondary β-TCP phase. Similar β-TCP stabilizing effect was previously reported for other smaller ions such as Mg and Zn [7, 43]. Moreover, when tried to prepare α-TCP containing 2 mol% of Mn, the annealed powders were just melted, probably due to formation of eutectic mixture.

FTIR spectroscopy was employed to further characterize the synthesized products and identify potential neighboring phases, which could be hardly detectable by XRD in the presence of major α-TCP phase. The FTIR spectra of α-TCP in the range from 400 to 1500 cm^{-1} are given in Fig. 2.

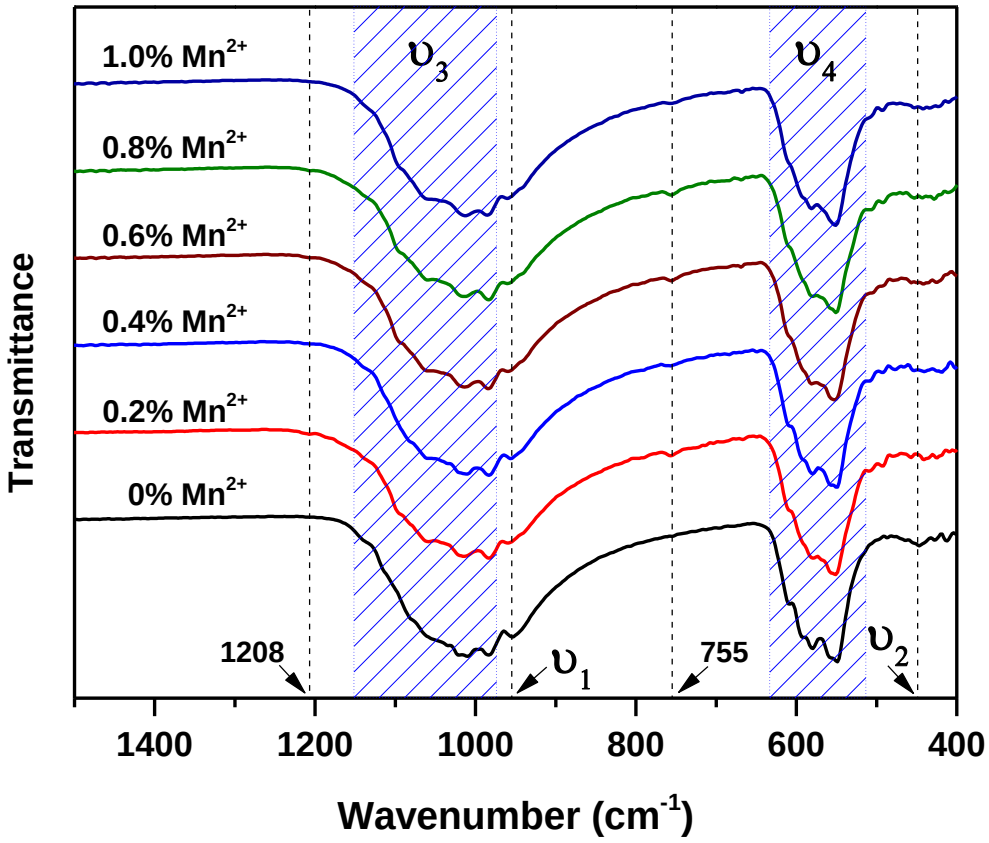

Fig. 2. FTIR spectra of α-TCP powders doped with different amounts of Mn^{2+}.

It is seen that all the obtained FTIR spectra are very similar and can be characterized by absorption bands characteristic of phosphate ions. The spectra are dominated by broad absorption bands located at 1150-970 cm^{-1} (υ_3), 550, 560, 582, 596 and 611 cm^{-1} (υ_4), 955 cm^{-1} (υ_1) and less intense band centered at 450 cm^{-1} (υ_2) [6]. The results confirm the formation of targeted α-TCP structure and shape of the spectra is very similar with that of previously reported FTIR spectra of α-TCP [6]. Nevertheless, additional very weak absorption bands, which do not correspond to α-TCP, were observed at 1208 and 755 cm^{-1}. These signals indicate the presence of negligible amount of calcium pyrophosphate ($Ca_2P_2O_7$) minor phase [44], which is quite often observed in TCP powders synthesized by precipitation method [31, 45, 46].

One of the most important steps in characterization of materials is to determine chemical composition of synthesized products. Moreover, it is known that in some cases the control of stoichiometry in mixed-cation compounds synthesized by co-precipitation method can be challenging. In order to confirm stoichiometric co-precipitation of both metal ions, elemental analysis by means of ICP-OES was performed. The results of the analysis are summarized in Table 1.

Table 1. Results of the elemental analysis of the samples performed by ICP-OES.

Sample	Mn/(Mn + Ca), mol%	(Mn + Ca)/P
$Ca_3(PO_4)_2$: 0% Mn^{2+}	-	1.46
$Ca_3(PO_4)_2$: 0.2% Mn^{2+}	0.21	1.47
$Ca_3(PO_4)_2$: 0.4% Mn^{2+}	0.42	1.47
$Ca_3(PO_4)_2$: 0.6% Mn^{2+}	0.62	1.47
$Ca_3(PO_4)_2$: 0.8% Mn^{2+}	0.82	1.47
$Ca_3(PO_4)_2$: 1.0% Mn^{2+}	1.01	1.50

It is obvious that determined Mn content is very close to theoretical values, which demonstrates that employed synthetic approach allows to prepare materials with controllable chemical composition. Total metals to phosphorous ratio shows slightly lower values than nominal 1.5:1. The possible explanation of insignificant deviation from theoretical values can be in the presence of minor $Ca_2P_2O_7$ phase, which was detected by FTIR spectroscopy.

X-band EPR spectra of the investigated samples are shown in Fig. 3 and representative Q-band EPR spectrum of TCP sample with 0.6 mol% of Mn^{2+} is presented in the inset of the figure.

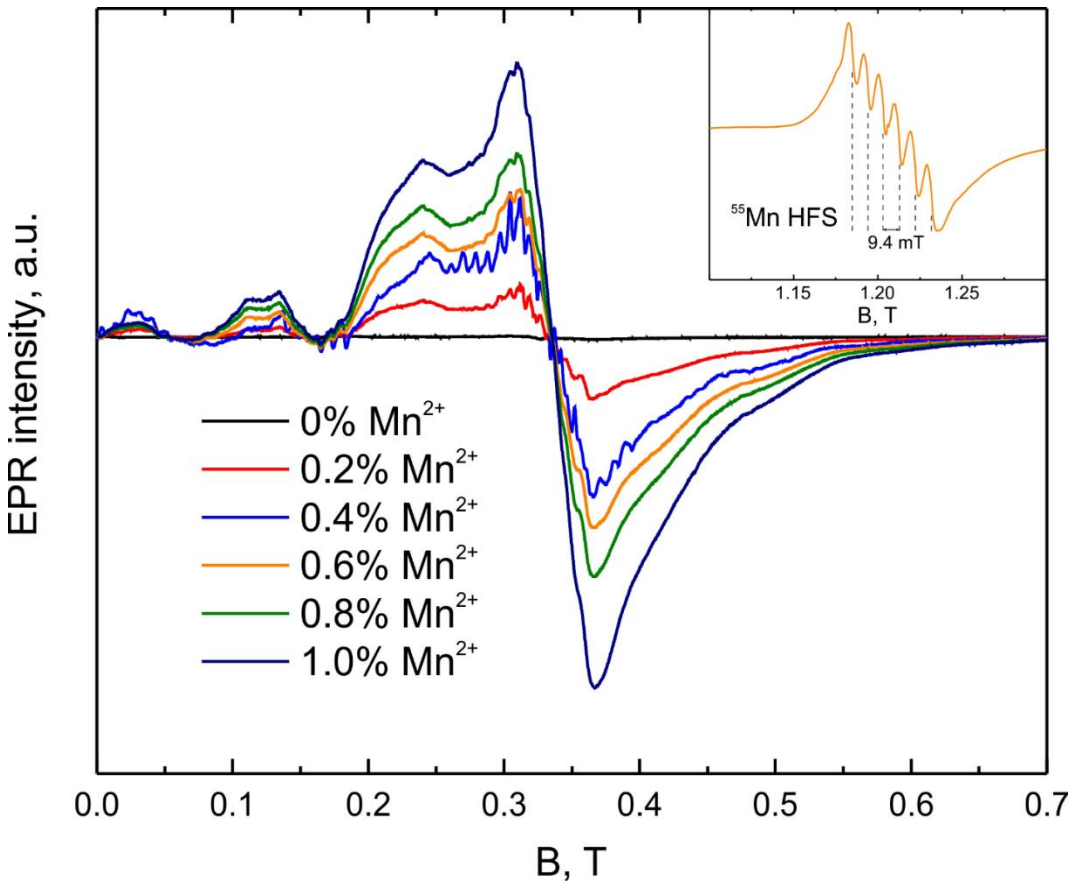

Fig. 3. Experimental X-band EPR spectra detected at room temperature. Inset: Q-band EPR spectrum of TCP sample with 0.6% Mn^{2+}.

EPR signals associated with Mn^{2+} are typical in the family of Mn-doped CPs [36, 39, 42, 47-53]. Mn^{2+} is an electron spin $S = 5/2$ paramagnetic system, which interacts with the 100% abundant ^{55}Mn isotope with nuclear spin $I = 5/2$. Zero field splitting (ZFS) of the ground state leads to five allowed transitions in the presence of external field B, which are further split into $2I+1 = 6$ hyperfine structure (HFS) components each. In powdered systems HFS is usually resolved for the central $m_S = -1/2 \leftrightarrow m_S = +1/2$ transition only, as the outer transitions are more sensitive to variations of ZFS parameter values induced by structural disorder effects. High field EPR can be used to simplify the spectra of high spin systems with a large magnitude of ZFS [36, 51], therefore measurements at Q-band were carried out. The additional spectra allowed to determine the average separation of

9.4 mT between the HFS components, which is close to the values reported for HAp and β-TCP [36, 39, 47-52]. Thus, it can be concluded that the coupling of Mn^{2+} electron and nuclear spins is similar for all these CPs.

The most apparent feature in X-band EPR spectra is the correlation of EPR signal intensities with the level of Mn doping. The double integral (DI) of EPR signal intensity is proportional to the number of spins in the sample and can be used for a quantitative analysis of Mn^{2+} content [51, 53]. An estimation of EPR spectra DI values normalized to the 1.0 mol% Mn^{2+} sample is given in Table 2. There is a reasonable correlation with the results of elemental analysis (see Table 1), which is a strong indication that Mn is predominantly in the 2+ oxidation state.

Table 2. Normalized DI values of EPR signal intensities for the investigated samples.

Sample	DI, arb.units
$Ca_3(PO_4)_2$: 0% Mn^{2+}	0.00
$Ca_3(PO_4)_2$: 0.2% Mn^{2+}	0.19
$Ca_3(PO_4)_2$: 0.4% Mn^{2+}	0.37
$Ca_3(PO_4)_2$: 0.6% Mn^{2+}	0.57
$Ca_3(PO_4)_2$: 0.8% Mn^{2+}	0.72
$Ca_3(PO_4)_2$: 1.0% Mn^{2+}	1.00

Apart from the broadening effect with an increase of Mn^{2+} concentration [36, 39, 42, 51-53] the shape of EPR spectra remains unchanged, which implies that ions occupy the same positions in the lattice up to 1.0 mol% substitution level. A notable exception is the TCP sample with 0.4 mol% of Mn^{2+}, for which sharp lines are overlaying the spectrum. The additional signal exhibits HFS characteristic to ^{55}Mn, therefore it must be originating from another Mn-related paramagnetic center. Mn^{2+} ions occupying other crystallographic sites of α-TCP structure or minor crystalline phases as well as Mn ions presenting in other oxidation states could be offered as possible explanations, however, additional studies are required to establish the nature of this phenomenon.

Fig. 4 shows SEM images of pristine and 1 mol% Mn^{2+}-doped α-TCP powders as representative.

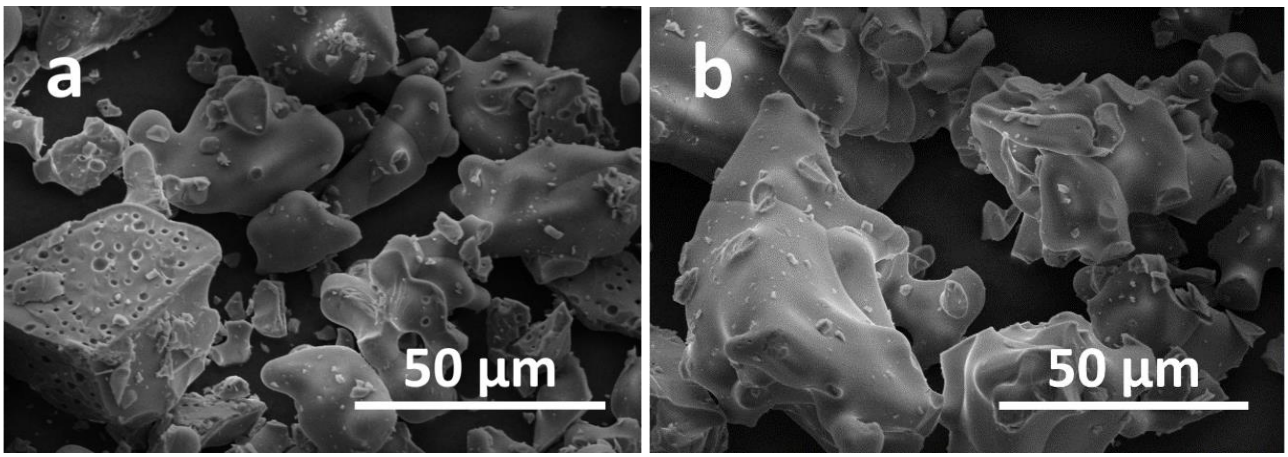

Fig. 4. SEM images of pristine (a) and 1 mol% Mn^{2+}-doped α-TCP (b) powders.

As it might be expected after annealing at high temperature and grinding in agate mortar, both samples consisted of the polydisperse monoliths of irregular shape. The size of the particles varied from approximately 5 to 80 µm. No clearly visible grains and grain boundaries were observed. Some pores can be seen on the interior surface of the crushed monoliths. Overall, there is no significant difference between pristine and doped samples indicating that in investigated doping level presence of Mn^{2+} ions does not have perceptible effect on morphology of α-TCP specimens.

Fig. 5 illustrates PL excitation and emission spectra of Mn^{2+}-doped α-TCP powders at room temperature.

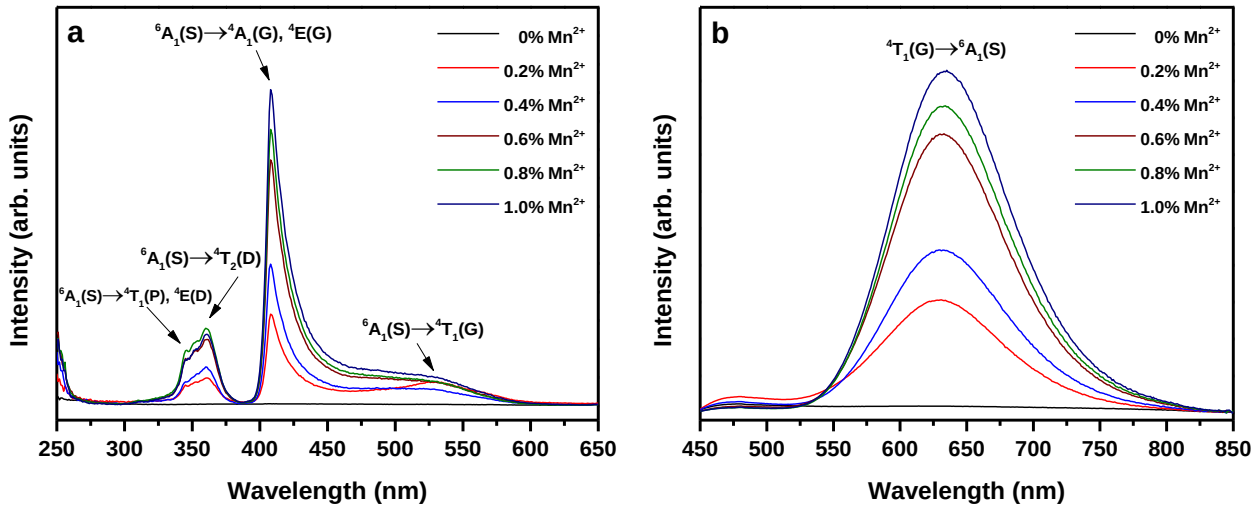

Fig. 5. Excitation (λ_{em} = 670 nm) and emission (λ_{ex} = 408 nm) spectra of Mn^{2+}-doped α-TCP.

Exploring the PL excitation spectra for 670 nm emission in the range from 250 to 650 nm (Fig. 5a), it is evident that undoped α-TCP sample is optically inactive. In the spectra of all Mn-doped samples few excitation bands centered at around 345, 360, 408 and 529 nm were clearly observed. These bands correspond to the transitions from the $^6A_1(S)$ level to the [$^4T_1(P)$, $^4E(D)$], $^4T_2(D)$, [$^4A_1(G)$, $^4E(G)$] and $^4T_1(G)$ levels, respectively. There is also one intense band at around 250 nm, which is caused by the charge transfer state of O^{2-}–Mn^{2+} transition [41, 54-56]. The shape of the excitation spectra is similar to that of previously reported for Mn^{2+}-doped β-TCP [42]. The PL emission spectra of the samples excited by 408 nm radiation possess a single broadband emission in the range of around 525–825 nm and centered at about 630 nm. Such emission spectrum is characteristic of a 3d-3d emission band of Mn^{2+} ions which is attributed to transition from exited $^4T_1(G)$ state to the fundamental $^6A_1(S)$ energy level [40-42]. All Mn-containing samples showed concentration-dependent behavior of both excitation and emission spectra. It is clearly seen that higher doping level results in stronger excitation and emission signals, the highest values were observed for α-TCP doped with 1 mol% of Mn^{2+} ions. However, as was mentioned above, we were not able to prepare α-TCP powders with higher Mn content in order to obtain higher emission intensity. The observed emission maximum is slightly blue-shifted in comparison to that of Mn-doped β-TCP and red-shifted compared to that of Mn-doped HAp, which were shown to be centered at 645 and 581 nm, respectively [42]. At the same time for X-ray excited Mn-doped β-TCP emission maximum was detected at 660 nm [38].

Fig. 6 shows decay curves of Mn^{2+}-doped α-TCP powders when specimens were excited at 408 nm and emission monitored at 630 nm. As observed, the decay curves are very similar regardless of Mn content in the samples. In order to calculate decay times, all obtained curves were fitted employing a two exponential decay function, since fitting by a single exponential function did not converge, resulting in a high chi-square values. The calculated decay constants τ revealed that the decay curves consist of initial fast decay process (τ_1) and a subsequent slow decay process (τ_2). The inset in Fig. 6 shows the mean values of decay constants as a function of Mn^{2+} concentration. It is seen that with an increase of Mn content the lifetime decreases, this dependence shows clearly linear behavior with an

exception for the sample containing 0.4 mol% of Mn^{2+}, which is obviously out of this trend. In order to correct this outlier, which we initially thought originates from a potential mistake in preparation of this particular sample, we additionally synthesized 5 separate α-TCP samples with 0.4 mol% of Mn. However, all extra syntheses were reproducible and showed same optical properties and lifetimes. Moreover, it goes hand in hand with additional signals in EPR spectra. Therefore, the reason of such anomalous behavior is unclear. Unfortunately, performed XPS analysis did not provide an information about the presence of other than Mn^{2+} valence states because of lack of sensitivity, since concentrations of Mn are quite low. Possible occupancy of another crystallographic site is also hardly provable because of the same reason and large number of Ca sites (18 inequivalent Ca sites) in α-TCP structure.

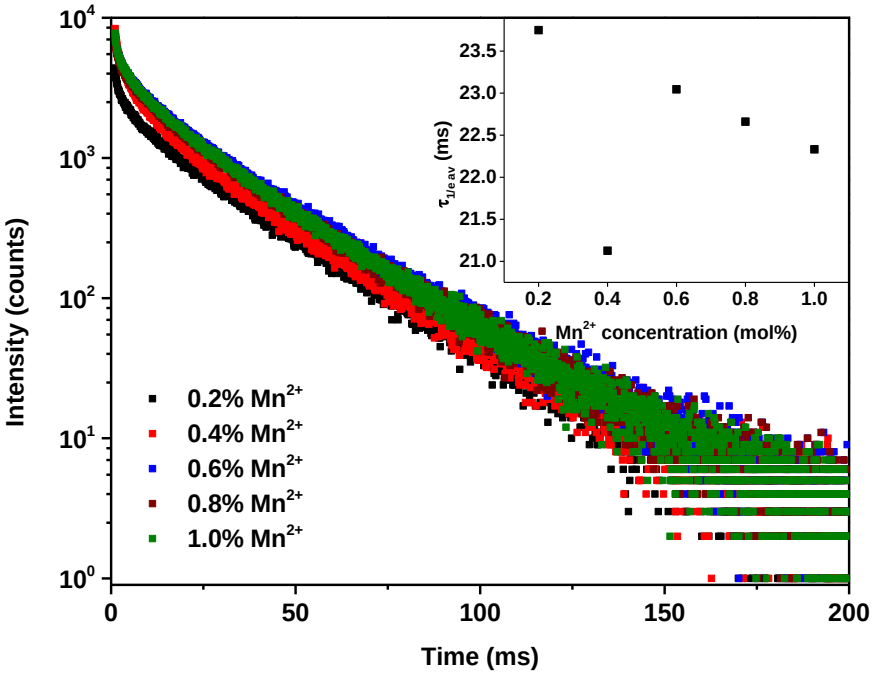

Fig. 6. PL decay (λ_{ex} = 408 nm, λ_{em} = 630 nm) curves of Mn^{2+}-doped α-TCP at room temperature. Inset: calculated decay constants.

The excitation and emission spectra of α-TCP doped with 1 mol% of Mn^{2+} are depicted in Fig. 7 as a function of temperature.

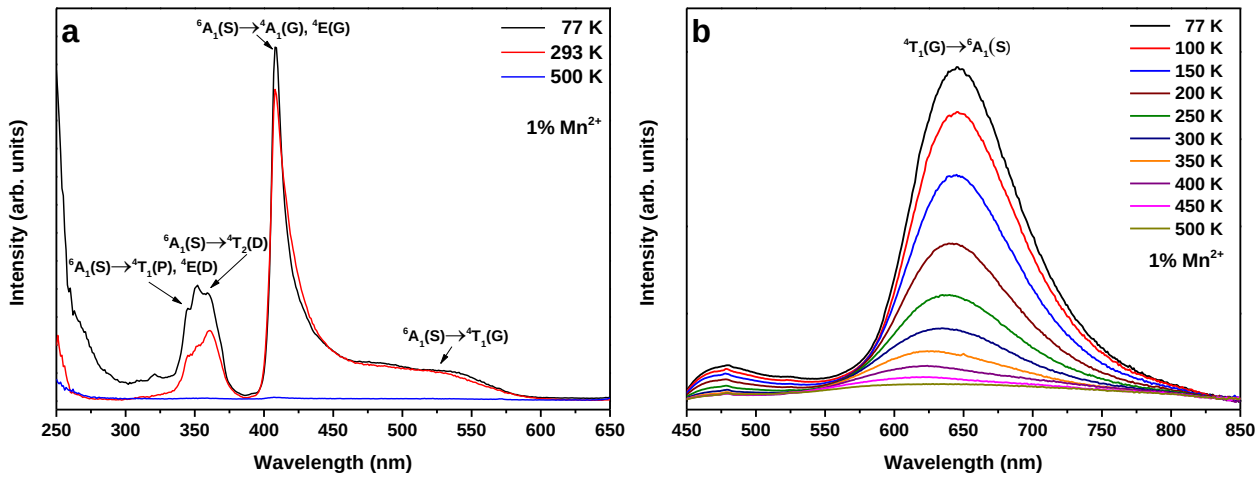

Fig. 7. Temperature-dependent excitation (λ_{em} = 670 nm) and emission (λ_{ex} = 408 nm) spectra of Mn^{2+}-doped α-TCP.

Evidently, the excitation spectrum changes significantly depending on the temperature (Fig. 7a). If compare the spectra at room temperature and at 77 K, it is seen that at lower temperature the intensity of excitation band corresponding to the charge transfer state of O^{2-}-Mn^{2+} transition and located at around 250 nm increases drastically. The intensity of the other bands in UV region also increases significantly, however in a longer wavelength region this increase is not so substantial. The intensity of excitation bands at 500 K is negligible compared to that at room temperature. It is also seen that emission intensity monotonically increases as temperature decreases (Fig. 7b), moreover a red shift was observed in the emission peak with decreasing temperature. It was found that emission peak gradually shifts from 620 nm at 500 K to 645 nm at 77 K. Another observed temperature-induced effect – emission peak broadening. It was determined that emission peak broadens significantly at elevated temperatures. This could be explained by the fact that at higher temperatures lattice vibrations increase leading to the changes in local surrounding of Mn^{2+} ions.

4. Conclusions

A series of Mn^{2+}-doped α-TCP powders with a doping level ranged from 0.2 to 1 mol% were successfully synthesized by co-precipitation method followed by high-temperature annealing and thermal quenching. The results of XRD, FTIR and elemental analysis confirmed that proposed synthetic approach is suitable for the synthesis of Mn^{2+}-doped α-TCP with a good phase purity and controllable chemical composition. Optical properties of the synthesized specimens were investigated in terms of PL. It was demonstrated that Mn-containing powders under excitation at 408 nm revealed a broadband emission in the range from 525 to 825 nm with a maximum centered at around 630 nm. Emission intensity was found to be dependent on concentration of Mn ions and increased as Mn content increased. On the contrary, PL lifetimes showed gradual decrease with an increase of Mn content. Temperature-dependent measurements of PL exhibited gradual and significant increase of emission intensity at lower temperatures.

Notes

The authors declare no competing financial interest.

Akcnowledgements

This project has received funding from European Social Fund (project No 09.3.3-LMT-K-712-19-0069) under grant agreement with the Research Council of Lithuania (LMTLT). Institute of Solid State Physics, University of Latvia as the Center of Excellence has received funding from the European Union's Horizon 2020 Framework Programme H2020-WIDESPREAD-01-2016-2017-TeamingPhase2 under grant agreement No. 739508, project CAMART². The World Federation of Scientists is highly acknowledged for the National Scholarship to AZ.

References

[1] W. Habraken, P. Habibovic, M. Epple, M. Bohner, Calcium phosphates in biomedical applications: materials for the future?, Mater. Today 19(2) (2016) 69-87.

[2] S.V. Dorozhkin, Calcium orthophosphates in nature, biology and medicine, Materials 2(2) (2009) 399-498.

[3] S.V. Dorozhkin, Functionalized calcium orthophosphates ($CaPO_4$) and their biomedical applications, J Mater Chem B 7(47) (2019) 7471-7489.

[4] M. Mathew, L.W. Schroeder, B. Dickens, W.E. Brown, The crystal structure of alpha-$Ca_3(PO_4)_2$, Acta Crystallogr. B 33(5) (1977) 1325-1333.

[5] B. Dickens, L.W. Schroeder, W.E. Brown, Crystallographic studies of the role of Mg as a stabilizing impurity in β-$Ca_3(PO_4)_2$. The crystal structure of pure β-$Ca_3(PO_4)_2$, J. Solid State Chem. 10(3) (1974) 232-248.

[6] R.G. Carrodeguas, S. De Aza, α-Tricalcium phosphate: Synthesis, properties and biomedical applications, Acta Biomater. 7(10) (2011) 3536-3546.

[7] M. Frasnelli, V.M. Sglavo, Effect of Mg^{2+} doping on beta-alpha phase transition in tricalcium phosphate (TCP) bioceramics, Acta Biomater. 33 (2016) 283-289.

[8] E. Boanini, M. Gazzano, A. Bigi, Ionic substitutions in calcium phosphates synthesized at low temperature, Acta Biomater. 6(6) (2010) 1882-1894.

[9] P.M.C. Torres, J.C.C. Abrantes, A. Kaushal, S. Pina, N. Döbelin, M. Bohner, J.M.F. Ferreira, Influence of Mg-doping, calcium pyrophosphate impurities and cooling rate on the allotropic α↔β-tricalcium phosphate phase transformations, J. Eur. Ceram. Soc. 36(3) (2016) 817-827.

[10] D. Brazete, P.M.C. Torres, J.C.C. Abrantes, J.M.F. Ferreira, Influence of the Ca/P ratio and cooling rate on the allotropic α↔β-tricalcium phosphate phase transformations, Ceram. Int. 44(7) (2018) 8249-8256.

[11] J.T. Zhang, F. Tancret, J.M. Bouler, Fabrication and mechanical properties of calcium phosphate cements (CPC) for bone substitution, Mater. Sci. Eng. C 31(4) (2011) 740-747.

[12] H. Ji, Z. Huang, Z. Xia, M.S. Molokeev, M. Chen, V.V. Atuchin, M. Fang, Y.g. Liu, X. Wu, Phase transformation in $Ca_3(PO_4)_2$:Eu^{2+} via the controlled quenching and increased Eu^{2+} content: Identification of new cyan-emitting α-$Ca_3(PO_4)_2$:Eu^{2+} phosphor, J. Am. Ceram. Soc. 98(10) (2015) 3280-3284.

[13] A. Bigi, E. Boanini, M. Gazzano, 7 - Ion substitution in biological and synthetic apatites, in: C. Aparicio, M.-P. Ginebra (Eds.), Biomineralization and Biomaterials, Woodhead Publishing, Boston, 2016, pp. 235-266.

[14] J.T.B. Ratnayake, M. Mucalo, G.J. Dias, Substituted hydroxyapatites for bone regeneration: A review of current trends, J. Biomed. Mater. Res. B: Appl. Biomater. 105(5) (2017) 1285-1299.

[15] T. Tite, A.-C. Popa, L.M. Balescu, I.M. Bogdan, I. Pasuk, J.M.F. Ferreira, G.E. Stan, Cationic Substitutions in Hydroxyapatite: Current Status of the Derived Biofunctional Effects and Their In Vitro Interrogation Methods, Materials 11(11) (2018) 2081.

[16] M. Šupová, Substituted hydroxyapatites for biomedical applications: A review, Ceram. Int. 41(8) (2015) 9203-9231.

[17] B. Yilmaz, A.Z. Alshemary, Z. Evis, Co-doped hydroxyapatites as potential materials for biomedical applications, Microchem. J. 144 (2019) 443-453.

[18] R. Meenambal, P. Poojar, S. Geethanath, S. Kannan, Substitutional limit of gadolinium in β-tricalcium phosphate and its magnetic resonance imaging characteristics, J. Biomed. Mater. Res. B: Appl. Biomater. 105(8) (2017) 2545-2552.

[19] S.S. Syamchand, G. Sony, Multifunctional hydroxyapatite nanoparticles for drug delivery and multimodal molecular imaging, Microchim. Acta 182(9) (2015) 1567-1589.

[20] C. Qi, J. Lin, L.-H. Fu, P. Huang, Calcium-based biomaterials for diagnosis, treatment, and theranostics, Chem. Soc. Rev. 47(2) (2018) 357-403.

[21] P. Mi, D. Kokuryo, H. Cabral, H. Wu, Y. Terada, T. Saga, I. Aoki, N. Nishiyama, K. Kataoka, A pH-activatable nanoparticle with signal-amplification capabilities for non-invasive imaging of tumour malignancy, Nat. Nanotechnol. 11(8) (2016) 724-730.
[22] L. Sinusaite, A. Popov, A. Antuzevics, K. Mazeika, D. Baltrunas, J.-C. Yang, J.L. Horng, S. Shi, T. Sekino, K. Ishikawa, A. Kareiva, A. Zarkov, Fe and Zn co-substituted beta-tricalcium phosphate (β-TCP): Synthesis, structural, magnetic, mechanical and biological properties, Mater. Sci. Eng. C 112 (2020) 110918.
[23] M. Gallo, B. Le Gars Santoni, T. Douillard, F. Zhang, L. Gremillard, S. Dolder, W. Hofstetter, S. Meille, M. Bohner, J. Chevalier, S. Tadier, Effect of grain orientation and magnesium doping on β-tricalcium phosphate resorption behavior, Acta Biomater. 89 (2019) 391-402.
[24] Y. Sogo, A. Ito, M. Kamo, T. Sakurai, K. Onuma, N. Ichinose, M. Otsuka, R.Z. LeGeros, Hydrolysis and cytocompatibility of zinc-containing α-tricalcium phosphate powder, Mater. Sci. Eng. C 24(6) (2004) 709-715.
[25] E. Boanini, S. Panzavolta, K. Rubini, M. Gandolfi, A. Bigi, Effect of strontium and gelatin on the reactivity of α-tricalcium phosphate, Acta Biomater. 6(3) (2010) 936-942.
[26] K. Hurle, J. Neubauer, F. Goetz-Neunhoeffer, Influence of Sr^{2+} on calcium-deficient hydroxyapatite formation kinetics and morphology in partially amorphized α-TCP, J. Am. Ceram. Soc. 99(3) (2016) 1055-1063.
[27] S.J. Saint-Jean, C.L. Camiré, P. Nevsten, S. Hansen, M.P. Ginebra, Study of the reactivity and in vitro bioactivity of Sr-substituted α-TCP cements, J. Mater. Sci. Mater. Med. 16(11) (2005) 993.
[28] D. Luo, C. Tong, Y. Zhu, C. Xu, Y. Li, Color tracing in the hydration process of α-$Ca_3(PO_4)_2$:Eu, J. Lumin. 219 (2020) 116863.
[29] W. Zhou, J. Han, X. Zhang, Z. Qiu, Q. Xie, H. Liang, S. Lian, J. Wang, Synthesis and photoluminescence properties of a cyan-emitting phosphor $Ca_3(PO_4)_2$:Eu^{2+} for white light-emitting diodes, Opt. Mater. 39 (2015) 173-177.
[30] C. Tong, Y. Zhu, C. Xu, L. Yang, Y. Li, Luminescence properties and color identification of Eu doped $Ca_3(PO_4)_2$ phosphors calcined in air, Physica B Condens. Matter 521 (2017) 153-157.
[31] P.M.C. Torres, S.I. Vieira, A.R. Cerqueira, S. Pina, O.A.B. da Cruz Silva, J.C.C. Abrantes, J.M.F. Ferreira, Effects of Mn-doping on the structure and biological properties of β-tricalcium phosphate, J. Inorg. Biochem. 136 (2014) 57-66.
[32] T. Wu, H. Shi, Y. Liang, T. Lu, Z. Lin, J. Ye, Improving osteogenesis of calcium phosphate bone cement by incorporating with manganese doped β-tricalcium phosphate, Mater. Sci. Eng. C 109 (2020) 110481.
[33] E. György, P. Toricelli, G. Socol, M. Iliescu, I. Mayer, I.N. Mihailescu, A. Bigi, J. Werckman, Biocompatible Mn^{2+}-doped carbonated hydroxyapatite thin films grown by pulsed laser deposition, J. Biomed. Mater. Res. A 71A(2) (2004) 353-358.
[34] R. Singh, M. Srivastava, N.K. Prasad, S. Awasthi, A. Kumar Dhayalan, S. Kannan, Structural analysis and magnetic induced hyperthermia of Fe^{3+} and Mn^{2+} substituted β-$Ca_3(PO_4)_2$, New J. Chem. 41(21) (2017) 12879-12891.
[35] Y. Huang, H. Qiao, X. Nian, X. Zhang, X. Zhang, G. Song, Z. Xu, H. Zhang, S. Han, Improving the bioactivity and corrosion resistance properties of electrodeposited hydroxyapatite coating by dual doping of bivalent strontium and manganese ion, Surf. Coat. Technol. 291 (2016) 205-215.
[36] J.V. Rau, I.V. Fadeeva, A.S. Fomin, K. Barbaro, E. Galvano, A.P. Ryzhov, F. Murzakhanov, M. Gafurov, S. Orlinskii, I. Antoniac, V. Uskoković, Sic Parvis Magna: Manganese-Substituted Tricalcium Phosphate and Its Biophysical Properties, ACS Biomater. Sci. Eng. 5(12) (2019) 6632-6644.
[37] Y.-j. Zhang, Z.-y. Mao, D.-J. Wang, J. Zhao, Synchronous red and blue emitting $Ca_3(PO_4)_2$:Eu^{2+}, Mn^{2+} phosphors applicable for plant-lighting, Mater. Res. Bull. 67 (2015) 1-4.
[38] A. Bessière, A. Lecointre, R.A. Benhamou, E. Suard, G. Wallez, B. Viana, How to induce red persistent luminescence in biocompatible $Ca_3(PO_4)_2$, J. Mater. Chem. C 1(6) (2013) 1252-1259.

[39] L. Sinusaite, A.M. Renner, M.B. Schuetz, A. Antuzevics, U. Rogulis, I. Grigoraviciute-Puroniene, S. Mathur, A. Zarkov, Effect of Mn doping on the low-temperature synthesis of tricalcium phosphate (TCP) polymorphs, J. Eur. Ceram. Soc. 39(10) (2019) 3257-3263.
[40] Q. Zhou, L. Dolgov, A.M. Srivastava, L. Zhou, Z. Wang, J. Shi, M.D. Dramićanin, M.G. Brik, M. Wu, Mn^{2+} and Mn^{4+} red phosphors: synthesis, luminescence and applications in WLEDs. A review, J. Mater. Chem. C 6(11) (2018) 2652-2671.
[41] G. Blasse, B.C. Grabmaier, A General Introduction to Luminescent Materials, Luminescent Materials, Springer Berlin Heidelberg, Berlin, Heidelberg, 1994, pp. 1-9.
[42] A. Lecointre, R. Ait Benhamou, A. Bessiére, G. Wallez, M. Elaatmani, B. Viana, Red long-lasting phosphorescence (LLP) in β-TCP type $Ca_{9.5}Mn(PO_4)_7$ compounds, Opt. Mater. 34(2) (2011) 376-380.
[43] L. Carbajal, A. Caballero, M.A. Sainz, Design and processing of ZnO doped tricalcium phosphate based materials: Influence of β/α polymorph phase assemblage on microstructural evolution, J. Eur. Ceram. Soc. 32(3) (2012) 569-577.
[44] B.C. Cornilsen, R.A. Condrate, The vibratonal spectra of β-$Ca_2P_2O_7$ and γ-$Ca_2P_2O_7$, J. Inorg. Nucl. Chem. 41(4) (1979) 602-605.
[45] L. Sinusaite, I. Grigoraviciute-Puroniene, A. Popov, K. Ishikawa, A. Kareiva, A. Zarkov, Controllable synthesis of tricalcium phosphate (TCP) polymorphs by wet precipitation: Effect of washing procedure, Ceram. Int. 45(9) (2019) 12423-12428.
[46] A. Destainville, E. Champion, D. Bernache-Assollant, E. Laborde, Synthesis, characterization and thermal behavior of apatitic tricalcium phosphate, Mater. Chem. Phys. 80(1) (2003) 269-277.
[47] I. Mayer, H. Diab, D. Reinen, C. Albrecht, Manganese in apatites, chemical, ligand-field and electron paramagnetic resonance spectroscopy studies, J. Mater. Sci. 28(9) (1993) 2428-2432.
[48] I. Mayer, F.J.G. Cuisinier, I. Popov, Y. Schleich, S. Gdalya, O. Burghaus, D. Reinen, Phase Relations Between β-Tricalcium Phosphate and Hydroxyapatite with Manganese(II): Structural and Spectroscopic Properties, Eur. J. Inorg. Chem. 2006(7) (2006) 1460-1465.
[49] I. Mayer, S. Cohen, S. Gdalya, O. Burghaus, D. Reinen, Crystal structure and EPR study of Mn-doped beta-tricalcium phosphate, Mater. Res. Bull. 43(2) (2008) 447-452.
[50] I. Matković, N. Maltar-Strmečki, V. Babić-Ivančić, M. Dutour Sikirić, V. Noethig-Laslo, Characterisation of β-tricalcium phosphate-based bone substitute materials by electron paramagnetic resonance spectroscopy, Radiat. Phys. Chem. 81(10) (2012) 1621-1628.
[51] F. Murzakhanov, G. Mamin, A. Voloshin, E. Klimashina, V. Putlyaev, V. Doronin, S. Bakhteev, R. Yusupov, M. Gafurov, S. Orlinskii, Conventional electron paramagnetic resonance of Mn^{2+} in synthetic hydroxyapatite at different concentrations of the doped manganese, IOP Conf. Ser. Earth Environ. Sci. 155 (2018) 012006.
[52] B. Sutter, T. Wasowicz, T. Howard, L.R. Hossner, D.W. Ming, Characterization of iron, manganese, and copper synthetic hydroxyapatites by electron paramagnetic resonance spectroscopy, Soil Sci. Soc. Am. J. 66(4) (2002) 1359-1366.
[53] B. Gabbasov, M. Gafurov, A. Starshova, D. Shurtakova, F. Murzakhanov, G. Mamin, S. Orlinskii, Conventional, pulsed and high-field electron paramagnetic resonance for studying metal impurities in calcium phosphates of biogenic and synthetic origins, J. Magn. Magn. Mater. 470 (2019) 109-117.
[54] L. Wu, B. Wang, Y. Zhang, L. Li, H.R. Wang, H. Yi, Y.F. Kong, J.J. Xu, Structure and photoluminescence properties of a rare-earth free red-emitting Mn^{2+}-activated $KMgBO_3$, Dalton Trans. 43(37) (2014) 13845-13851.
[55] L. Lin, M. Yin, C. Shi, W. Zhang, Luminescence properties of a new red long-lasting phosphor: Mg_2SiO_4:Dy^{3+}, Mn^{2+}, J. Alloys Compd. 455(1) (2008) 327-330.
[56] R. Cao, W. Wang, J. Zhang, Y. Ye, T. Chen, S. Guo, F. Xiao, Z. Luo, Luminescence properties of $Sr_2Mg_3P_4O_{15}$:Mn^{2+} phosphor and the improvement by co-doping Bi^{3+}, Opt. Mater. 79 (2018) 223-226.

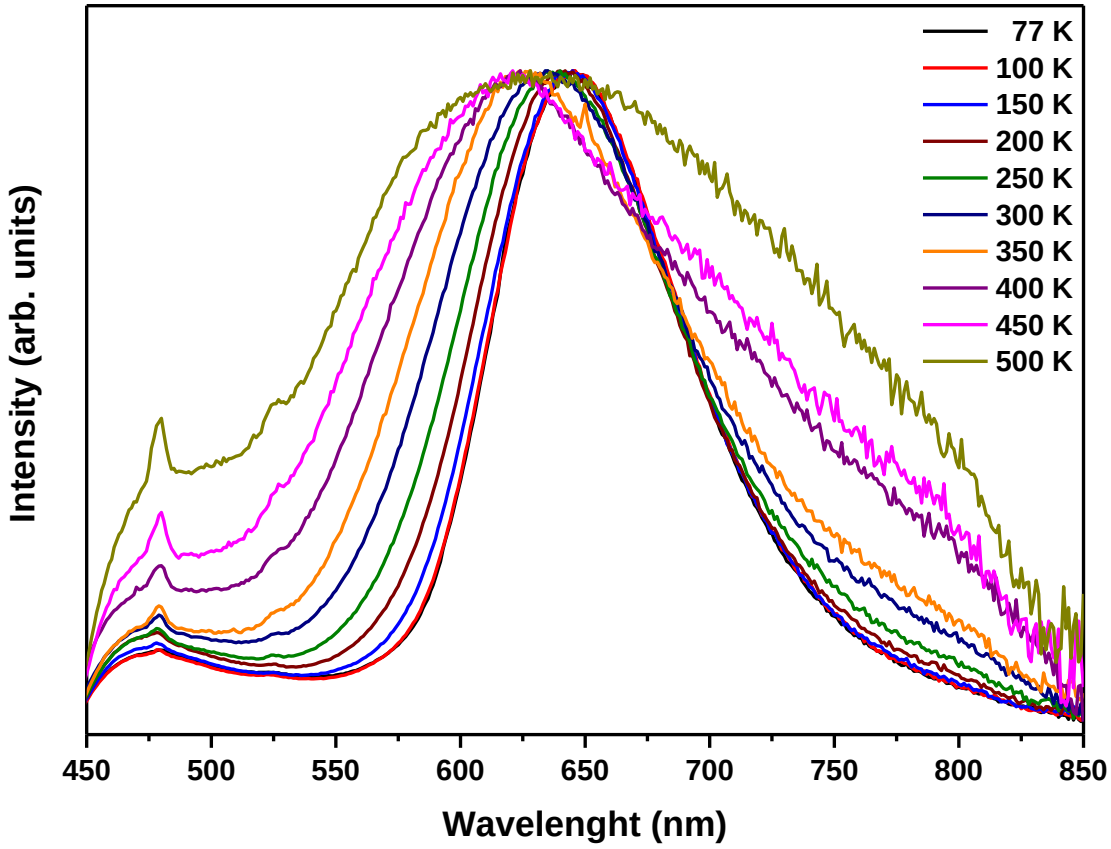

447

448 **Fig. 7b** . Normalized emission spectra (will not be shown)

449

Supporting Information (maybe will not be included)

Synthesis, structural and luminescent properties of Mn-doped alpha-tricalcium phosphate

Lauryna Sinusaite[1], Andris Antuzevics[2], Anatoli I. Popov[2], Uldis Rogulis[2], Martynas Misevicius[1], Arturas Katelnikovas[1], Aivaras Kareiva[1], Aleksej Zarkov[1,*]

[1]*Institute of Chemistry, Vilnius University, Naugarduko 24, LT-03225 Vilnius, Lithuania*

[2]*Institute of Solid State Physics, University of Latvia, Kengaraga 8, LV-1063 Riga, Latvia*

*Corresponding author: E-mail: aleksej.zarkov@chf.vu.lt; +37062190153.

Table S1. PL lifetime values of Mn-doped α-TCP (λ_{em} = 630 nm, λ_{ex} = 408 nm)

Mn, mol%	τ_1, ms	τ_2, ms	$\tau_{vid.}$, ms
0.2	6.97	26.78	23.749
0.4	**5.19**	**25.14**	**21.126**
0.6	6.83	26.06	23.045
0.8	6.98	25.78	22.661
1.0	6.66	25.49	22.332